Journal of Zhejiang University SCIENCE A
ISSN 1009-3095 (Print); ISSN 1862-1775 (Online)
www.zju.edu.cn/jzus; www.springerlink.com
E-mail: jzus@zju.edu.cn

An edge-preserving algorithm of joint image restoration and volume reconstruction for rotation-scanning 4D echocardiographic images*

GUO Qiang, YANG Xin

(*Institute of Image Processing and Pattern Recognition, Shanghai Jiao Tong University, Shanghai 200030, China*)

E-mail: guoqiang1221@sjtu.edu.cn; yangxin@sjtu.edu.cn

Received Aug. 5, 2005; revision accepted Mar. 28, 2006

Abstract: A statistical algorithm for the reconstruction from time sequence echocardiographic images is proposed in this paper. The ability to jointly restore the images and reconstruct the 3D images without blurring the boundary is the main innovation of this algorithm. First, a Bayesian model based on MAP-MRF is used to reconstruct 3D volume, and extended to deal with the images acquired by rotation scanning method. Then, the spatiotemporal nature of ultrasound images is taken into account for the parameter of energy function, which makes this statistical model anisotropic. Hence not only can this method reconstruct 3D ultrasound images, but also remove the speckle noise anisotropically. Finally, we illustrate the experiments of our method on the synthetic and medical images and compare it with the isotropic reconstruction method.

Key words: Echocardiography, Image reconstruction, Anisotropic
doi:10.1631/jzus.2006.A0960 **Document code:** A **CLC number:** TP391

INTRODUCTION

3D echocardiography has been widely used in diagnostic cardiology because it can visualize the complex structure of heart more accurately than previous used 2D diagnosis method. Currently, there are two major image acquisition methods of 3D echocardiography, i.e., random data acquisition and sequential data acquisition (Roelandt, 2000). The former uses a spatial locator to measure the position and orientation of the ultrasound probe, allowing unrestricted (free-hand) scanning from any available precordial acoustic window. It is usually adopted to assess the structure and surface shapes and to analyze the left ventricular volume quantitatively. In our work, 3D echocardiography is applied to analyze the abnormality of the mitral valve, which causes complex congenital heart disease. In this application, rotational scanning, one mode of sequential data acquisition, is used to acquire the ultrasound images. This approach is shown in Fig.1. The end-firing endocavity probe is put on the region near the heart (Fig.1a). The stepper-motor is fixed on the probe handle and is directly controlled by the images acquisition system. This motor rotates the transducer in the tip of the probe at predetermined increments over a span of 180°. It results in sequential 2D images collected from the same pivot point and at equal interval angles to one another. With this method, 10~20 2D images are acquired within one cardiac cycle, encompassing systole and diastole at each position of the transducer. Therefore, the acquired images are time series of 3D echocardiographic images, i.e., 4D images. Each 3D ultrasound image represents a state of heart at one time instant during the cardiac cycle (Fig.1b). The acquired images intersect each other along a revolution axis forming a cylindrical geometry, which may be used to reconstruct the 3D structure of the heart (Fig.1c).

There are two distinct reconstruction approaches

* Project supported by the National Basic Research Program (973) of China (No. 2003CB716104), and Shanghai Science and Technology Research Foundation (No. 034119820), China

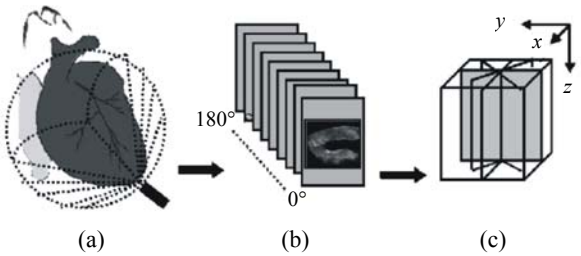

Fig.1 Rotation-scanning approach with end-firing probe. (a) Image acquiring procedure; (b) The acquired images; (c) 3D reconstruction using acquired images

(Fenster *et al*., 2001): feature-based and voxel- based reconstruction. In the feature-based approach, the desired features (e.g., contours or surfaces) of anatomical structures are first determined and then reconstructed into a 3D image. The second approach is based on using a set of acquired 2D images to build a voxel-based image, i.e., a regular Cartesian grid of volume elements in three dimensions. For each 3D image point, the voxel value (intensity) is calculated by interpolation, as the weighted average of the pixel values of its nearest neighbors among the embedded 2D image pixels. Ghosh *et al*.(1982) carried out a study on 3D reconstruction of cylindrical echocardiographic images. Following his work, many different interpolation methods were proposed. For example, Nearest-neighbor interpolation, linear interpolation and bilinear interpolation were used in (Tong *et al*., 1996). Concentric interpolation was introduced by Duann *et al*.(1999). The warped distance interpolation may also be implemented to enhance the quality of reconstructed volume (Ramponi, 1999). Moreover, the statistical method formulated in Bayesian framework may also be applied in the interpolation (Tsai *et al*., 1993).

Sanches and Marques (2000) introduced a Bayesian approach to reconstruct the 3D ultrasound images, using Rayleigh distribution as the observation model. Not only can this approach reconstruct the 3D volume, but also remove the speckle noise simultaneously. Based on the same framework, Sanches and Marques (2003) proposed a statistical approach to compensate the misalignment and geometric distortions of the acquisition images. These artifacts are unavoidable during the image acquisition process (Tong *et al*., 1998; Cardinal *et al*., 2000; Treece *et al*., 2001). Supplemental work would be required to deal with artifacts before reconstruction if we adopt the traditional method. Furthermore, Sanches and Marques (2001) proposed a fast algorithm to speed up the procedure of solving those problems. However, their work is based on the images acquired by free-hand method, which is quite different from the rotation scanning method geometrically. Inspired by their work, we present an anisotropic 3D reconstruction and restoration algorithm designed for rotation-scanning ultrasound images. First, an MAP-MRF based reconstruction method is established to reconstruct 3D volume, using the images acquired by rotational scanning method. Then the spatio-temporal nature of ultrasound images is introduced for the selection of parameter α in the energy function. Parameter α is the measurement of the strength of the connection between neighborhood nodes. Hence this reconstruction model is anisotropic, which avoids blurring the boundary during the reconstruction process.

The paper is organized as follows: Section 2 presents the volume reconstruction model for cylindrical echocardiographic images. Section 3 contains the parameter formulation, explaining how to obtain parameter α. Section 4 shows experimental results for verifying the proposed method and Section 5 concludes the paper.

RECONSTRUCTION MODEL

As proposed by Sanches and Marques (2000), in the method of voxel-based 3D reconstruction, the 3D space is divided into cubic cells, forming 3D regular grid (Fig.2). One cubic cell is shown in Fig.3a. Its value is the weighted average of the pixel values of its

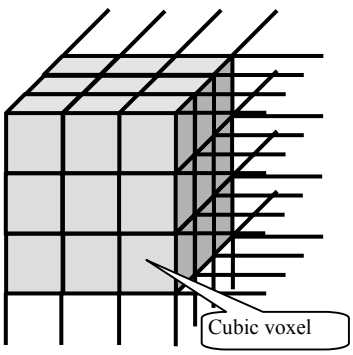

Fig.2 3D space is divided into cubic cells, forming the cubic regular grid

nearest neighbors, i.e., u_1, u_2, …, u_8 (Fig.3a). Hence the intensity of a voxel may be considered to be the value of function $f(x)$, i.e.,

$$f(x)=\boldsymbol{B}(x)^{\mathrm{T}}\boldsymbol{U}, \tag{1}$$

where $\boldsymbol{B}(x)=\{b_s(x)\}$ is a vector of basis functions and $\boldsymbol{U}=\{u_s\}$ (s=1, 2, …, 8) is a vector of unknown coefficients to be estimated. It is assumed that each $b_s(x)$ is a basis function obtained by shifting the tri-linear interpolation function (Sanches and Marches, 2000).

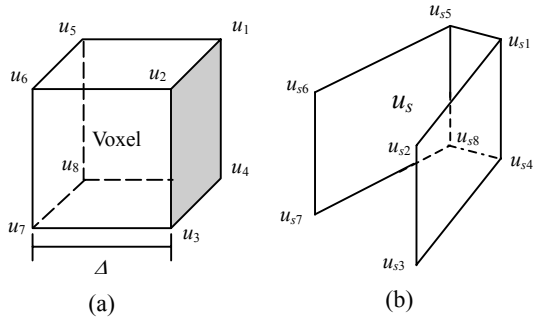

Fig.3 (a) One voxel in the cubic regular grid. Each neighbor of the voxel can be calculated according to the structure shown in (b)

Since the given images intersect each other along a revolution axis, the value of u_s can be calculated according to the structure shown in Fig.3b. u_{s1}, u_{s2}, u_{s3}, u_{s4} are on one piece of 2D ultrasound image and u_{s5}, u_{s6}, u_{s7}, u_{s8} are on the other. There is angular slice spacing between the two adjacent 2D ultrasound images. These eight nodes compose the finite support region. How to estimate u_s from those known nodes is the key step in the reconstruction.

One challenge for ultrasound images volume reconstruction is that those given images are noise contaminated. Hence, using such images directly to reconstruct the volume may cause degraded results. Usually, noise reduction precedes the job of traditional volume reconstruction methodologies. However, the distribution of speckle noise can be embodied in some statistical reconstruction model. In this paper, Maximum A posteriori Probability (MAP) estimation was implemented, i.e.,

$$\hat{\boldsymbol{U}} = \arg\max_{\boldsymbol{U}} \ln p(\boldsymbol{U} \mid \boldsymbol{Y}), \tag{2}$$

where $\boldsymbol{Y}=(y_i, x_i)$ is the available data, y_i is the intensity of location x_i, $\boldsymbol{U}$ is the vector of u_s.

Applying Bayes rule, Eq.(2) can be rewritten as:

$$\hat{\boldsymbol{U}} = \arg\max_{\boldsymbol{U}} \ln[p(\boldsymbol{Y} \mid \boldsymbol{U})p(\boldsymbol{U})], \tag{3}$$

where $p(\boldsymbol{Y}|\boldsymbol{U})$ is the likelihood function and $p(\boldsymbol{U})$ is the prior. Formulation of these two terms is as follows.

The speckle noise that contaminated the ultrasound images is introduced by the interaction of acoustic wave with the tissues and the ultrasound probe surface during the image acquisition. The analysis of the physics associated with the ultrasound propagation and the interaction with the tissues suggest that the pixel value (i.e. intensity) variations of ultrasound image can be approximated by Rayleigh distribution (Shankar, 1986; Corsine *et al*., 1996). Furthermore, the pixel value (i.e. intensity) can be considered as realization of independent random variables with Rayleigh distribution. So the likelihood function can be written as:

$$p(\boldsymbol{Y} \mid \boldsymbol{U}) = \prod_i \frac{y_i}{f(x_i)} \exp\left[-\frac{y_i^2}{2f(x_i)}\right], \tag{4}$$

where $f(x_i)$ is the value of the function $f(x)$ to be reconstructed at x_i .

The interpolation information is included in the prior $p(\boldsymbol{U})$. According to the spatial properties of human organs and tissues, a Gibbs prior is used (Li, 2001). The adoption of a Gibbs distribution is equivalent to considering $\boldsymbol{U}$ as Markov Random Field (MRF) according to the interpretation of Hammersley-Clifford theorem (German and German, 1984). So the prior distribution can be given by:

$$p(\boldsymbol{U})=Z^{-1}\cdot \mathrm{e}^{-E(\boldsymbol{U})}, \tag{5}$$

where Z is a normalization factor and $E(\boldsymbol{U})$ is the energy function. Adoption of this prior is equivalent to considering the neighboring should have similar values.

The energy function in prior is a sum of clique potential over all possible cliques.

$$E(\boldsymbol{U}) = \alpha \sum_{p\in G} \sum_{i\in N(p)} (u_p - u_i)^2, \tag{6}$$

where G denotes the grid nodes and $N(p)$ are the neighbors of the pth node on the given 2D images.

$$p(\boldsymbol{U}) = Z^{-1} \cdot \exp\left[-\alpha \sum_{p \in G} \sum_{i \in N(p)} (u_p - u_i)^2\right]. \quad (7)$$

The neighborhood system and clique is defined on the irregular sites (Fig.4). Each grid node is connected to eight neighbors, except the boundary nodes. The parameter α measures the strength of each connection and plays a very important role in the reconstruction algorithm. Discussion about the parameter α is shown in Section 3.

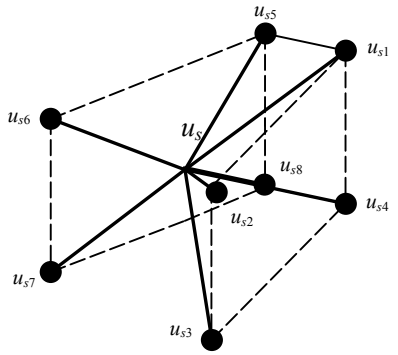

Fig.4 Clique and neighbor system

MAP criteria require the maximization of the joint density $L(\boldsymbol{U})$ with respect to $\boldsymbol{U}$.

$$L(\boldsymbol{U}) = \ln p(\boldsymbol{Y}, \boldsymbol{U}) = \ln p(\boldsymbol{Y} \mid \boldsymbol{U}) p(\boldsymbol{U})$$
$$= \ln\left\{\prod_i \left[\frac{y_i}{f(x_i)} e^{y_i^2/(2f(x_i))}\right] \frac{1}{Z} e^{-\alpha \sum_{(i,j)} (u_i - u_j)^2}\right\}. \quad (8)$$

Iterated Conditional Model (ICM) algorithm (Besag, 1986) is used to solve the problem of the maximization of $L(\boldsymbol{U})$ with respect to $\boldsymbol{U}$, which leads to

$$u_s = \frac{1}{4\alpha N} \sum_i \frac{y_i - 2f(x_i)}{f^2(x_i)} b_p(x_i) + \overline{u}_s, \quad (9)$$

where u_s is the intensity of a grid node, N is the number of neighbors of u_s and $\overline{u}_s$ denotes the average intensity of the neighbors of u_s. Eq.(9) suggests an iterative procedure to compute u_s.

PARAMETER FORMULATION

The adoption of Gibbs distribution in the prior introduces the regularization while searching for a global minimum and converts the objective function into a non-convex one. So, general method cannot guarantee obtaining the global solution. Therefore, the careful selection of statistical parameter in prior plays a very important role. The bigger the value of parameter α is, the lower the convergence rate of the algorithm is, because an increased dependence is enforced among neighboring nodes. Therefore the parameter α cannot remain constant during the optimization process, or the algorithm will be trapped in a local minimum, far from the desired solution. Sanches and Marques (2002) obtained the parameter α by trial and error, and showed how it changes during the 3D reconstruction process. However if the parameters used to estimate the coefficient vector are constant, the reconstruction model will be isotropic, and may result in blurred boundary in the estimated volume. It will make the succeeding segmentation of the mitral valve very difficult.

On the other hand, parameter α reflects the intensity difference between the neighboring nodes. A high value of α corresponds to a strong connection between two neighboring nodes, while low values of α corresponds to weak connections. In this paper, we take into account the connection strength of the nodes for the selection of parameter α, in addition to its influence on the convergence of the algorithm.

The strength of connection between neighboring nodes can be measured by spatial gradient. A large spatial gradient represents weak connection, which often occurs in the area of the boundary; while small value of gradient represents strong connection of neighboring nodes, which indicates the local smoothness. Furthermore, the acquired images are time sets of data. So the temporal consistency can be also introduced to the selection of parameter α. The formulation of the selection of parameter α is shown as:

$$\alpha = \alpha_{\text{ini}} \beta, \quad (10)$$

where α_{ini} is the initial value resulting in the isotropic volume; β is the adaptative factor, whose value is the

result of penalty function $S(x)$ which may be defined as:

$$\beta = S(x) = \begin{cases} \operatorname{arc\,cot}(x-\eta)+\pi, & x<\eta, \\ \operatorname{arc\,cot}(x-\eta), & x \geq \eta, \end{cases} \tag{11}$$

where η is a large positive constant, which is the mean value of the gradient of some sample points on the border. The plot of penalty function is shown in Fig.5. The penalty function input value is the gradient measurement, represented by the x-axis in Fig.5; the y-axis of the function plot represents the adaptative factor that is the output value of the penalty function. The reasons for choosing such penalty function are as follows: First, the penalty function is a monotonously decreasing function, as large as the gradient measurement and as small as the adaptative factor, i.e., the value of the adaptative factor is in inverse proportion to the value of gradient measurement. Second, this function is centrosymmetric; the position of centre is determined by parameter η, which can be specified appropriately according to the quality of the given images. The value of η will influence the clarity of the boundary of the reconstructed images, which is illustrated in Section 4. Third, this penalty function has two horizontal asymptotes, which limit the variational scope of the adaptative factor value. Finally, the function curve indicates that the nearer is the distance to the centre point, the steeper is the function curve, which enhances the boundary of the reconstructed volume.

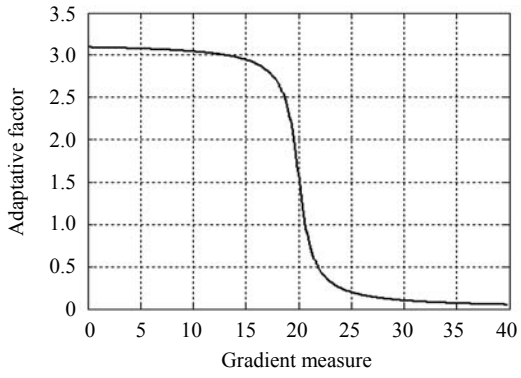

Fig.5 Plot of penalty function

The gradient measurement is given by $g(x,y,z,t)$:

$$g(x,y,z,t)=\boldsymbol{E}\cdot[\boldsymbol{D}\nabla I(x,y,z,t)], \tag{12}$$

where $\boldsymbol{E}=\{1,1,1,1\}$, $I(x,y,z,t)$ is the 3D ultrasound image at instant t. $\boldsymbol{D}$ denotes the anisotropic tensor which can be written as:

$$\boldsymbol{D}=\operatorname{diag}\left(k\left(\frac{\partial I}{\partial x},\delta_x\right),k\left(\frac{\partial I}{\partial y},\delta_y\right),k\left(\frac{\partial I}{\partial z},\delta_z\right),k\left(\frac{\partial I}{\partial t},\delta_t\right)\right), \tag{13}$$

where $k(x,\delta)$ is the diffusion function (Weickert, 1998). δ denotes the gradient threshold. This function has the effect of reducing the diffusion at 'high' gradients, based on a threshold δ.

From Eqs.(12) and (13), we can deduce the following expression:

$$\begin{aligned} g(x,y,z,t) = {} & k\left(\frac{\partial I}{\partial x},\delta_x\right)\frac{\partial I}{\partial x}+k\left(\frac{\partial I}{\partial y},\delta_y\right)\frac{\partial I}{\partial y} \\ & +k\left(\frac{\partial I}{\partial z},\delta_z\right)\frac{\partial I}{\partial z}+k\left(\frac{\partial I}{\partial t},\delta_t\right)\frac{\partial I}{\partial t}. \end{aligned} \tag{14}$$

The expression above is discretized by the finite differences method. Since the given nodes are on the irregular grid, we approximate the partial differential as follows:

$$\frac{\partial I}{\partial x}=\left\|\frac{1}{4\Delta_x}\left[(u_{i1}+u_{i2}+u_{i5}+u_{i6})-(u_{i3}+u_{i4}+u_{i7}+u_{i8})\right]\right\|, \tag{15.1}$$

$$\frac{\partial I}{\partial y}=\left\|\frac{1}{4\Delta_y}\left[(u_{i1}+u_{i2}+u_{i3}+u_{i4})-(u_{i5}+u_{i6}+u_{i7}+u_{i8})\right]\right\|, \tag{15.2}$$

$$\frac{\partial I}{\partial z}=\left\|\frac{1}{4\Delta_z}\left[(u_{i2}+u_{i3}+u_{i6}+u_{i7})-(u_{i1}+u_{i4}+u_{i5}+u_{i8})\right]\right\|, \tag{15.3}$$

$$\frac{\partial I}{\partial t}=\left\|\frac{1}{8\Delta_t}\left(\sum_{j=1}^{8}u_{ij}^{t+1}-\sum_{j=1}^{8}u_{ij}^{t}\right)\right\|, \tag{15.4}$$

where u_{ij}^t denotes the intensity of node u_{ij} at instant t; Δ_x, Δ_y and Δ_z are grid steps in three directions. Δ_t is the time step.

For each wedged grid, Eq.(9) is implemented to calculate the coefficient u_s. Before this iterative procedure, parameter α may be obtained by the approach

presented above. Then, it is reduced gradually during the iterative process as shown in (Sanches and Marques, 2002). The variation of parameter α during the process of reconstruction is shown in Fig.6.

EXPERIMENTAL RESULTS

In the experiment, the reconstruction algorithm with constant parameters for all coefficients estimation and the algorithm proposed in this paper are named as isotropic reconstruction method and anisotropic reconstruction method, respectively.

Experiments were composed of three parts: Part 1 compares the reconstructed volumes from isotropic reconstruction method with anisotropic reconstruction method on synthetic images and medical images; Part 2 calculates and compares the signal to noise ratio (SNR) of reconstructed volume from those two kinds of reconstruction method; Part 3 illustrates the function of parameter η in the penalty function.

Comparison of reconstructed volumes from two methods

The synthetic data consists of a set of 60 images of 128×128 pixels, each of which intersects each other along a revolution axis. The angular slice spacing of adjacent images is 3°. One of those images is shown in Fig.7a. It is blurred by Gaussian low pass filter and contaminated by the speckle noise. So, all those synthetic images simulate the real ultrasound images acquired by rotational scanning method.

A grid of 127×127×127 nodes was used in the test. Experimental results are shown in Fig.8, left images of each group are the results of isotropic reconstruction method; right images of each group are from anisotropic approach. Both 3D reconstructed volumes are shown in Fig.8a. In order to make the difference between the two results more visible, two cross-sections are extracted from the estimated volume respectively, as shown in Fig.8b. Moreover, Fig.8c shows the surface plots of these two cross-sections. Those figures prove that our reconstruction method has edge-preserving ability.

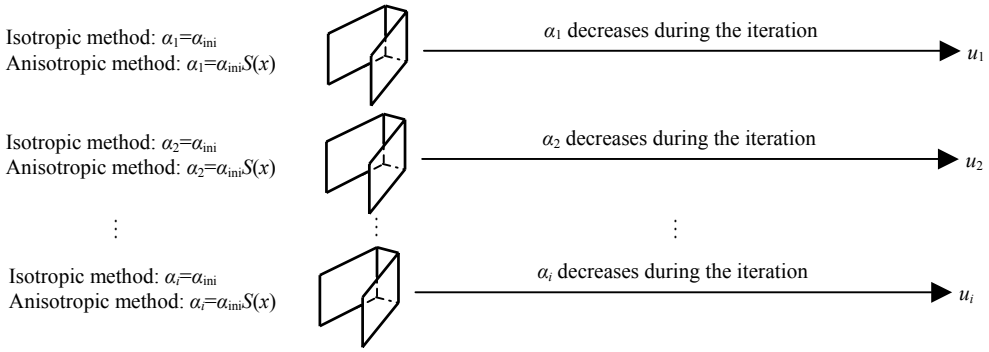

Fig.6 Given the structure shown in Fig.3b, each coefficient u_i can be calculated by an iteration process indicated by Eq.(9). The parameter α decreases during the iteration and avoids trapping in a local minimum. The initial values of all parameter α in the isotropic reconstruction method are the same, i.e., $\alpha_1=\alpha_2=\ldots=\alpha_{ini}$. However, in the anisotropic reconstruction method, each parameter α is different, i.e., $\alpha_i=\alpha_{ini}S(x)$, where $S(x)$ is penalty function. α_{ini} can be obtained by trial and error

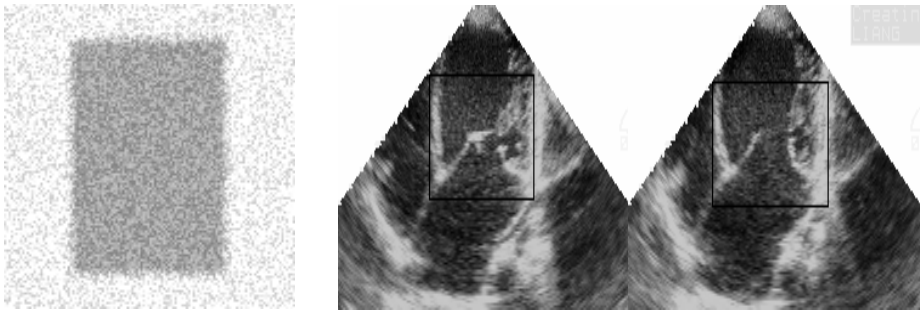

(a) (b)

Fig.7 Source images: synthetic images and medical images. (a) Synthetic image; (b) Real ultrasound images

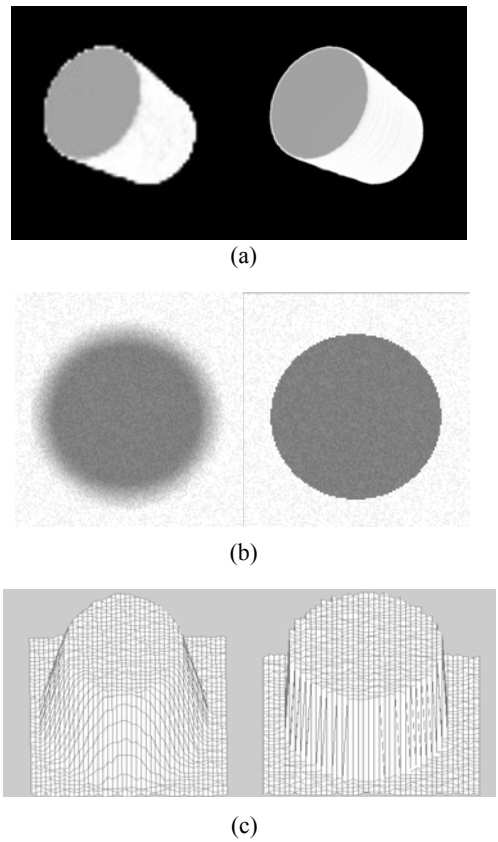

Fig.8 Comparison between isotropic and anisotropic reconstruction methods on synthetic images. (a) Reconstructed 3D volume; (b) Cross-sections extracted from 3D volume; (c) Surface-plot of cross-sections

Similar experiments were performed with the medical images, which were acquired by Philips Sonos 5500 using TTO probe. The first two frames of source images are shown in Fig.9. Those two figures are adjacent images with 3° angular spacing. Since reconstructing the whole images consume much time, we only reconstructed the region of interest with black rectangle as shown in Fig.9b, i.e., the mitral valve.

A grid of 84×84×84 nodes was chosen to reconstruct the volume. A comparison of estimated volume between two algorithms is shown in Fig.9. Left images of each group are the results of isotropic reconstruction method; right images of each group are from anisotropic approach. The two reconstructed volumes are shown in Fig.9a. 3D reconstruction is the precondition for the segmentation of the mitral valve. Fig.9b shows two cross-sections extracted from the estimated volume. Two groups of surface plots of those two cross-sections are shown in Figs.9c and 9d respectively, indicating the difference between the two methods. They are viewed from different angles.

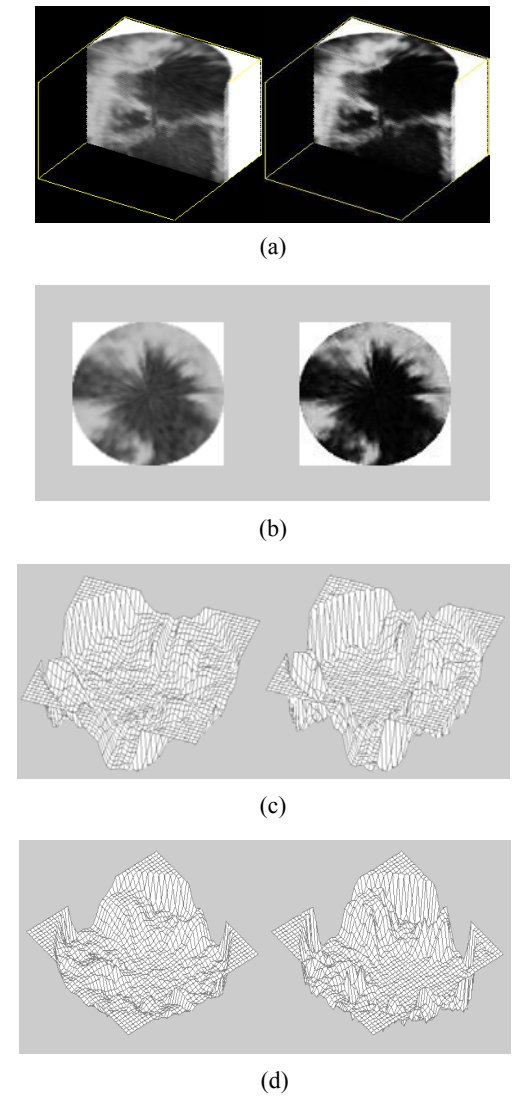

Fig.9 Comparison between isotropic and anisotropic reconstruction methods on medical images. (a) Reconstructed 3D volume; (b) Cross-sections extracted from 3D volume; (c) Surface-plot of cross-sections; (d) Surface-plot of cross-sections from a different angle

The computer used to reconstruct the 3D volumes is HP workstation xw4100. Synthetic images reconstruction and medical image reconstruction cost about 57 s and 34 s respectively.

SNR comparison of the two reconstruction methods

In this test, the results were evaluated according to objective criteria and by visual inspection. Signal to noise ratio (SNR) was used to evaluate the estimated volume:

$$SNR = 10\lg \frac{\int |f_0(x)|\,\mathrm{d}x}{\int |f(x) - f_0(x)|\,\mathrm{d}x}, \qquad (16)$$

where $f_0(x)$ denotes the true data on image intensity. $f(x)$ denotes the reconstructed image intensity. *SNR* was computed based on Fig.8b (synthetic images) and Fig.9b (medical images). As to the medical images, $f_0(x)$ was obtained through averaging of a series of images acquired at the same location. Comparison of *SNR* between two algorithms showed in Table 1 indicates that the anisotropic reconstruction algorithm not only results in an edge-preserving volume, but also removes the noise more effectively.

Table 1 SNR comparison between isotropic (iso.) and anisotropic (aniso.) reconstruction methods

Image	*SNR*	
	Aniso. algorithm	Iso. algorithm
Synthetic	22.4	17.6
Medical	21.3	19.8

Discussion of parameter η in the penalty function

As stated in Section 3, the value of η in the penalty function influences the quality of reconstructed volume. First, its value can be initialized by the gradient of a point at the boundary on the given images. Then we adjust it by trial and error. Too larger or too smaller than the appropriate value blur the boundary. Fig.10 shows anisotropic reconstructed methods whose η adopted three different values. Left images of the three groups are cross sections extracted from the reconstructed volume from the same position. The other two images are surface plots of the cross section from different view angles. Fig.10a shows the results using η=75; Figs.10b and 10c are results obtained by using η=58 and η=90 respectively. These results indicate that different values of η can influence the definition of the reconstructed volume because the value of η determines the center position of the penalty function.

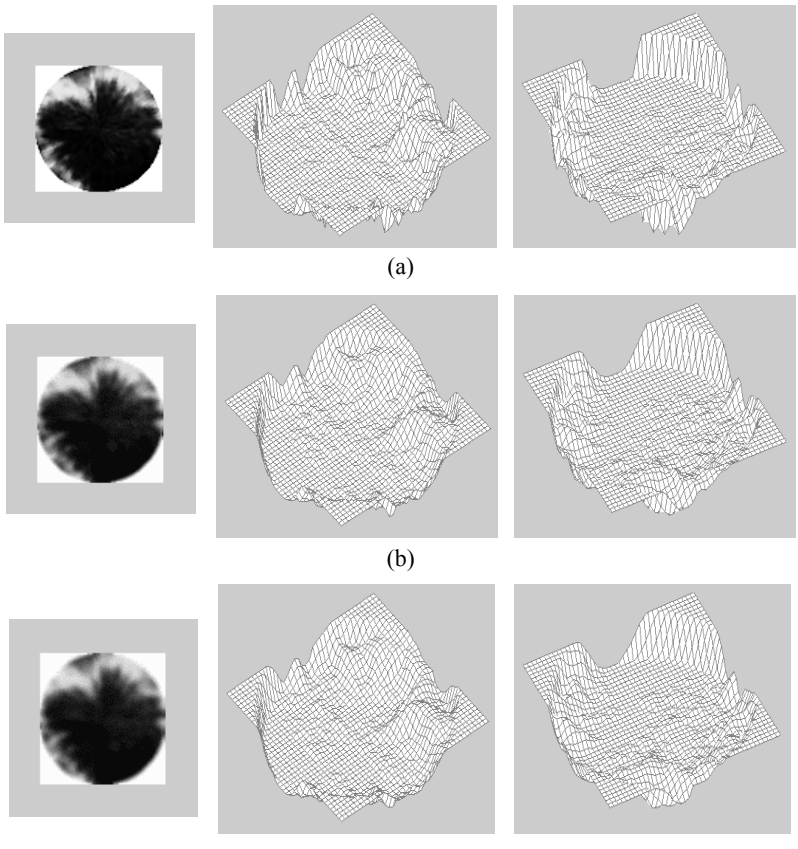

Fig.10 Reconstruction results using different values of parameter η. (a) η=75; (b) η=58; (c) η=90

CONCLUSION

3D reconstruction and restoration is a very important step in the quantitative analysis of mitral valve defect. In this paper, we propose an anisotropic algorithm based on MAP-MRF for this purpose. There are three advantages of this method. First, the anisotropic property, which results in a clear boundary in the estimated volume, benefits the following segmentation step in our work. Second, the statistical method can also be easily extended to deal with the misalignment and geometric distortions in the echocardiograpic images. Third, during the process of 3D reconstruction, the speckle noise can be removed effectively; it is supported by the adoption of Rayleigh distribution in the likelihood function.

Several research directions can be explored in the future. First, optimizing the velocity of the reconstruction process is one of them. Although the algorithm can be linearized to speed up the reconstruction process (Sanches and Marches, 2001), it is still far from the real-time requirement. Second, extending the method introduced in this paper to deal with the artifacts is another direction. A third direction concerns the choice of penalty function. The penalty function adopted in this paper may not be the best one. How to choose a penalty function according to the source images is an interesting question. Finally, parameters simplification is another direction worth exploring. Many parameters in the reconstruction model need to be specified. It is expected that some simple principles need to be explored to reduce the unknown parameters.

ACKNOWLEDGEMENT

The ultrasound images were kindly provided by YAO Linping from Xinhua Hospital attached to Shanghai Second Medical University.

References

Besag, J., 1986. On the statistical analysis of dirty pictures. *J. Roy. Statist. Soc.*, *Ser.B*, **48**(3):259-302.

Cardinal, H.N., Gill, J., Fenster, A., 2000. Analysis of geometrical distortion and statistical variance in length, area and volume in a linearly scanned 3D ultrasound image. *IEEE Trans. Med. Imaging*, **19**(6):632-651. [doi:10.1109/42.870670]

Corsine, G., Mossa, A., Verrazzani, L., 1996. Signal-to-noise ratio and autocorrelation function of the image intensity in coherent systems: sub-Rayleigh and super-Rayleigh conditions. *IEEE Trans. Image Process*, **5**(1):132-141. [doi:10.1109/83.481677]

Duann, J.R., Lin, S.B., Hu, W.C., Su, J.L., 1999. Computer system for four-dimensional transesophageal echocardiographic image reconstruction. *Computerized Medical Imaging and Graphics*, **23**(4):173-179. [doi:10.1016/S0895-6111(99)00016-6]

Fenster, A., Downey, D.B., Cardinal, H.N., 2001. Three-dimensional ultrasound imaging. *Phys. Med. Biol.*, **46**(5):67-99. [doi:10.1088/0031-9155/46/5/201]

German, S., German, D., 1984. Stochastic relaxation, gibbs distributions, and the Bayesian restoration of images. *IEEE Trans. Pattern Analysis and Machine Intelligence*, **6**:721-741.

Ghosh, A., Nanda, N.C., Maurer, G., 1982. Three-dimensional reconstruction of echocardiographic images using the rotation method. *Ultrasound in Med. & Bio.*, **8**(6):655-657. [doi:10.1016/0301-5629(82)90122-3]

Li, S.Z., 2001. Markov Random Field Modeling in Computer Vision, 2nd Ed. Springer-Verlag, p.37-63.

Ramponi, G., 1999. Warped distance for space-variant linear image interpolation. *IEEE Trans. Image Processing*, **8**(5):629-639. [doi:10.1109/83.760311]

Roelandt, Jos R.T.C., 2000. Three-dimensional echocardiography: the future today! *Computers & Graphics*, **24**(5):715-729. [doi:10.1016/S0097-8493(00)00074-1]

Sanches, J.M., Marques, J.S., 2000. A Rayleigh reconstruction/interpolation algorithm for 3D ultrasound. *Pattern Recognition Letter*, **21**(10):917-926. [doi:10.1016/S0167-8655(00)00053-2]

Sanches, J.M., Marques, J.S., 2001. A Fast MAP Algorithm for 3D Ultrasound. EMMCVPR 2001, p.63-74.

Sanches, J.M., Marques, J.S., 2002. A multiscale algorithm for three-dimensional free-hand ultrasound. *Ultrasound Med. & Biol.*, **28**(8):1029-1040. [doi:10.1016/S0301-5629(02)00548-3]

Sanches, J.M., Marques, J.S., 2003. Joint image registration and volume reconstruction for 3D ultrasound. *Pattern Recognition Letter*, **24**(4-5):791-800. [doi:10.1016/S0167-8655(02)00182-4]

Shankar, P., 1986. Speckle reduction in ultrasound B-scans using weighted averaging in spatial compounding. *IEEE Trans. Ultrasonic, Ferroelectrics and Frequency Control*, **33**(6):754-758.

Tsai, C.J., Hung, Y.P., Hsu, S.C., 1993. Comparison between Asymptotic Bayesian Approach and Kalman Filter-Based Technique for 3D Reconstruction Using an Image Sequence. CVPR, p.206-211.

Tong, S., Downey, D.B., Cardinal, H.N., Fenster, A., 1996. A three-dimensional ultrasound prostate imaging system. *Ultrasound Med. & Biol.*, **22**(6):735-746. [doi:10.1016/0301-5629(96)00079-8]

Tong, S., Cardinal, H.N., Downey, D.B., Fenster, A., 1998. Analysis of linear, area and volume distortion in 3D ultrasound imaging. *Ultrasound Med. & Biol.*, **24**(3):355-373. [doi:10.1016/S0301-5629(97)00268-8]

Treece, G.M., Prager, R.W., Gee, A.H., Berman, L., 2001. Correction of Probe Pressure Artifacts in Freehand 3D Ultrasound. Proceeding of Medical Image Computing and Computer-Assisted Intervention (MICCAI 2001), p.283-290.

Weickert, J., 1998. Anisotropic Diffusion in Image Processing. Teubner Verlag, p.54-107.